Inverted human umbilical arteries with tunable wall thicknesses for nerve regeneration

Thomas Crouzier, Trosper McClendon, Zehra Tosun, Peter S. McFetridge
School of Chemical, Biological and Materials Engineering, The University of Oklahoma Bioengineering Center, University of Oklahoma, 100 East Boyd Street, Norman, Oklahoma 73019-1004

Received 25 August 2007; revised 18 January 2008; accepted 12 February 2008
Published online 9 July 2008 in Wiley InterScience (www.interscience.wiley.com). DOI: 10.1002/jbm.a.32103

Abstract: Tubular nerve guides have shown a potential to bridge nerve defects, by directing neuronal elongation, localizing growth factors, and inhibiting fibrotic cellular ingrowth. These investigations describe a novel acellular scaffold derived from the human umbilical cord artery that aims to enhance nerve regeneration by presenting a unique mechanical and chemical environment to the damaged nerve ends. A rapid, semiautomated dissection technique is described that isolates the human umbilical artery (HUA) from the umbilical cord, after which the vessel is decellularized using sodium dodecyl sulfate (SDS). The artery is turned inside out to produce a 3D scaffold, that unlike previous vessels for nerve repair, is more resistant to collapse. The scaffold has the potential as either an acellular bridge-implant, or for *in vitro* nerve regeneration. Stress–strain relationships and suture retention were assessed to determine whether the material had similar mechanical properties to native nerves. A dual process-flow perfusion bioreactor was developed to assess glucose mass transfer, and to investigate the culture of neuronal-like PC12 cells within the scaffold. These investigations have shown the automated dissecting method yields a smooth tubular scaffold, where wall thickness can be tuned to alter the mechanical behavior of the scaffold. Inverting the scaffold prevents collapse, with the decellularized iHUA having comparable mechanical properties to native nerves. Bioreactor cultures with PC12 cells seeded within iHUA lumenal void were shown to adhere and migrate into the preexisting ECM after 11 days of culture. These investigations show the potential of the iHUA as a unique 3D scaffold that may enhance nerve regeneration.
 J Biomed Mater Res 89A: 818–828, 2009

Key words: umbilical artery; tissue engineering; nerve; nerve guide

INTRODUCTION

In the United States, more than 50,000 surgical procedures are carried out to repair peripheral nerves annually. In addition to loss of function and disability; treatment costs have a significant economical impact.[1,2] As a result, research efforts toward developing efficient repair techniques to bridge severed nerves are actively sort. Earlier techniques, such as end-to-end microsutures, were shown to improve nerve function; however, autograft harvesting and relocation remains the "gold standard" for clinical treatment. Although these treatments have been successful over smaller defects, there remains a clinical need to bridge larger defects, and minimize the need to use autologous tissue in which secondary injuries are induced.

Correspondence to: P. S. McFetridge; e-mail: pmcfetridge@ou.edu

Tubular guidance channels have had some success with smaller defects by providing a supportive matrix that prevents fibrous tissue infiltration, and allows growth factors secreted by the nerve stumps to be concentrated to promote axonal elongation.[3] The tissue engineering approaches aims to further improve regeneration, by implanting partially (or wholly) grown *neo*-nerve tissue to bridge the defect. Current materials can be grouped into several distinct categories; autologous tissue grafts, nonautologous tissue and acellular grafts, natural-based materials, and synthetic materials. Although significant progress has been made in recent years, little is known of the regenerative process, due predominantly to the complexity of healing phenomena. This problem has been attenuated by the difficulty in recreating the wound in an artificial environment to facilitate our understanding of these biological processes. However, identifying ideal materials that promote nerve regeneration without undesirable side effects remains an active area of research.

Previous investigations have shown the utility of nonnervous autologous tissue grafts. In particular,

vein grafts have been shown to be effective at bridging small nerve defects in animal models[4,5] and in humans.[6] However, these unmodified veins were prone to collapse, especially in longer sections, and the presence of valves was occasionally shown to block axonal elongation.[7,8] A modification of this technique introduced by Wang et al., turned the vein inside–out, in which the normal structure of the material is inverted to compact the adventitial layer in the core of the inverted vessel.[9] Turning the vessel inside out was shown to reduce vessel collapse, with a further perceived advantage of exposing a rich collagenous matrix to the regenerating axons.[9–11] Although this technique showed promise, it was not as successful as hoped, with some published data finding no significant difference between standard and inside–out veins.[12,13] Arteries were first successfully used as nerve guides by Bungner in 1891.[14] Although chemically similar to veins, several physical characteristics such as wall thickness, permeability, and mechanical rigidity differ. Rat aortic arteries have been used for peripheral nerve repair in several studies, yielding heterogeneous but satisfactory results.[15]

Materials suitable as 3D scaffold for nerve tissue engineering applications must meet a number of criteria in order to be successful. Ideally, scaffolds need to be biocompatible, able to withstand physiological stresses without structural failure, with a tubular lumen conducive to neuronal growth. Importantly, scaffolds that enclose cellular components must not limit mass-transfer of nutrients and waste products whereby inhibiting the grafts regenerative potential.

As the popularity of *ex vivo* tissues continues to grow as scaffold for tissue regeneration, methods of isolating and preparing the tissues continue to be optimized for improved performance. In these investigations, modified human umbilical arteries (HUA) have been assessed as a novel 3D scaffold for nerve tissue engineering applications. As a progression to optimize the tissue as a nerve conduit, a novel mechanical dissection technology has been used to isolates the artery from the umbilical cord, allowing vessels with different wall thicknesses to be prepared, followed by decellularization using sodium dodecyl sulfate (SDS). By varying the wall thickness, the inside–out HUA (iHUA) can be engineered to provide more, or less, area for cell growth within the *neo*-lumen as well as reducing the potential for tissue collapse by compressing the glycoprotein-rich Wharton's jelly within the lumen. Mechanical analysis and preliminary cellular interactions with the scaffold have been assessed, showing promising results, that coupled with a unique glycoprotein-rich extracellular matrix (ECM) may provide enhanced nerve regeneration.

EXPERIMENTAL METHODS

Cell culture

PC12 neuronal-like cells were cultured in standard T75 tissue culture flasks and maintained with Dulbecco's modified eagle medium (DMEM; Invitrogen, Carlsbad, CA) supplemented with 10% heat inactivated fetal calf serum (Atlanta Biologicals, Norcross, GA), 86 μg/mL penicillin, and 86 μg/mL streptomycin (Invitrogen), at 37°C, 5% CO_2. Media were refreshed every 3 days.

Automated dissection of the HUA

Human umbilical cords collected from a local hospital within 24 h of delivery. Cords were stored for a maximum of 3 days at 5°C before use. Cords were first cleaned of blood and cut into 11 cm sections. A 2-mm diameter glass rod was then inserted into the vessel lumen to slightly stretch the artery wall allowing insertion of the machining mandrel (3.10 mm OD stainless steel). Mounted cords were then rolled in paper towels, placed within a polystyrene container, and frozen to −80°C for a minimum of 12 h to ensure a homogeneous temperature throughout the cord. Mounted cords were removed from the −80°C freezer and immediately inserted into the bench-top lathe (Central Machinery, Mod 33647, China) and secured. The cutting tool was set to the appropriated cutting thickness (0.25, 0.50, or 0.75 mm) and secured. A rotational speed of 2900 rpm was set and the linear drive engaged at a cutting rate of 5 mm/s. Machined tissue was thawed at 5°C, then cut into 5-cm long sections prior to use.

Decellularization and inversion of the HUA

iHUA segments were immersed in a 1% (w/v) SDS solution for 24 h and shaken at 100 rpm on an orbital shaker. Tissue sections were then rinsed (three times) in distilled water and washed for 24 h in 75% (v/v) ethanol to remove the amphiphilic surfactant molecule and aid lipid extraction.[16] Three final washes were performed with deionized water before being stored in PBS at 4°C. All treatment/washing solutions were maintained at a ratio of 100 mL per vessel to ensure an adequate diffusion gradient. Once decellularized the HUA was turned inside–out using a set of arthroscopy forceps. Forceps were inserted through the artery lumen, clamped to the distal end, then withdrawn back through the vessel pulling the distal end through the lumen. HUA were then referred as inside out HUA (iHUA).

Bioreactor and process flow

Threaded glass tubes (×2) with a diameter of 12 mm were used to construct the bioreactors (Kimble Kontes no. 671780-0013, Vineland, NJ). End caps with silicone sealing rings screwed over the glass tubes to seal the system around the inlet and outlet adapters. Adapters connected

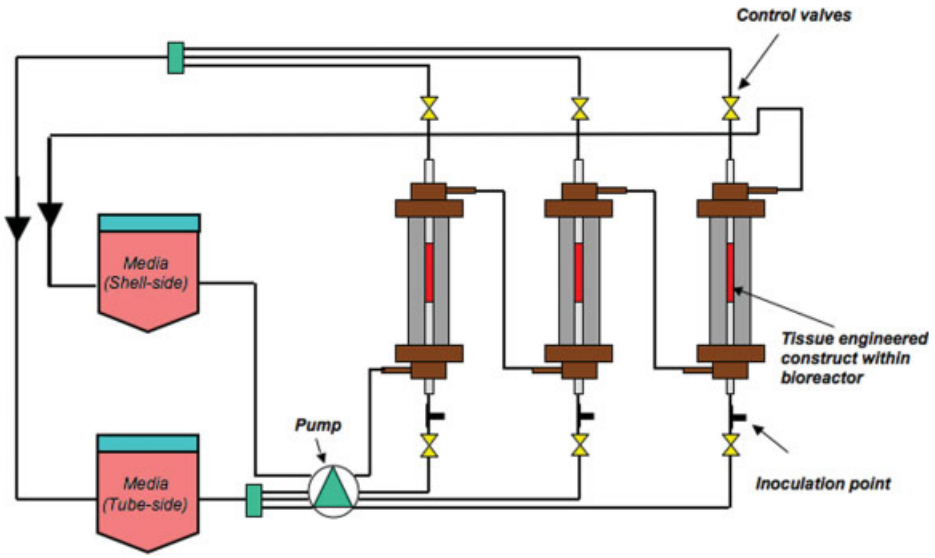

Figure 1. Bioreactor process flow: The process flow allows independent flow separation between the lumenal (tube-side) and ablumenal (shell-side), with three bioreactors. Ablumenal flow was in-series to deliver media to the construct during the culture period, with lumenal flow in-parallel. Lumenal perfusion only during scaffold sterilization only, with cell seeding as a direct inoculation of cells into the central void of the scaffold. Once seeding was complete the lumenal circuit was closed and media was perfused through the ablumenal flow circuit only. [Color figure can be viewed in the online issue, which is available at www.interscience.wiley.com.]

the scaffold at the distal and proximal ends allowing flow though the interior of the scaffold (tube-side flow), with inlet and outlet glass ports fused to the exterior of the bioreactors main body providing ablumenal flow (shell-side). The setup for perfusion culture used three bioreactors, connected by 1.6-mm silicon tubing (Masterflex LS14, Cole-Parmer, IL) to a multi cartridge peristaltic pump (Masterflex 7550-50, pump head 7519-06, cartridge 7519-70) and a media reservoir. The ablumenal flow circuits were connected in series, with the lumenal flow connected in parallel. Shut-off valves were placed at either end of each bioreactor to isolate the lumen once the scaffolds were seeded, see Figure 1.

Bioreactor assembly and cell seeding

The iHUA was attached to stainless steel inlet/outlet adapters (2.4 mm IO, 3.3 mm OD) using plastic zip ties, then inserted into the bioreactor and sealed. Prior to cell seeding, scaffolds were sterilized by perfusing both shell and tube-side flow circuits with 0.1% peracetic acid in 4% ethanol for 2 h.[17–19] The pH of the arteries was adjusted to 7.2 by flushing with PBS for 2 h then with DMEM overnight. The flow rate was set at 2 mL/min for all preseeding solutions. PC12 cells were prepared as a homogenous solution to a final density of 1.5×10^6 cell/mL within a 20-mL sterile syringe. Bioreactors were sequentially seeded by connecting the syringe directly to a three-way leur adapter located at the proximal end of each bioreactors tube-side inlet port. Bioreactors were maintained in a vertical orientation to expel air as the cell suspension was inoculated into the lumen. Once loaded the distal valve was closed, then a minimal amount of pressure to ensure the scaffold was completely full; at which point the proximal valve was closed isolating the lumen of the scaffolds. Media was perfused only through the shell-side circuit (2 mL/min) during the culture phase. Complete systems were maintained at 37°C, 5% CO_2 for 2 weeks with 100% media changes every 3 days. The same settings were used to assess cellular glucose consumption inside the artery as a function of time. A 10 μL sample was removed from the ablumenal system and glucose concentration was measured using a hexokinase-glucose 6-phosphate dehydrogenase based assay (G3293, Sigma, St. Louis, MO) and measuring absorbance at 340 nm to determine glucose concentration.

ANALYTICAL METHODS

Mechanical testing

A uniaxial tensile testing rig (United Testing Systems, model SSTM-2K, Flint, MI) was used to determine stress–strain relationships, Young's modulus, and yield stress. For longitudinal tensile analysis, arteries were dissected into flat sheets (~10 mm wide × 30 mm long), and clamped at the proximal and distal ends. Samples were then preloaded to a stress of 0.05 N at a rate of 5 mm/min,[20] then elongated until failure at 5 mm/min.

Material stiffness was calculated at both the linear and nonlinear regions of the stress strain curve. Peripheral nerves are typically subjected to strain values between 10 and 30% elongation, from this region a linear regression was performed, and the stiffness was deduced from the slope. Stiffness in the toe region was used to calculate the

point of inflexion, meaning the point of transition between the two distinctly different stiffness regions of the biphasic material. The section of strain between 0 and 10% of the curve was fitted with a fourth degree polynomial and the roots of the second derivative calculated yielding the point of inflexion in percent strain. The slope of the data point situated between 0% strain and the point of inflexion was then calculated to obtain the "toe region" stiffness.

Suture holding capacity was assessed by applying uniaxial stress to sutured samples (United Testing Systems). Arterial sections were cut longitudinally to form a 10 mm wide $\times$ 30 mm long sheet, a single sterile 3-0 braided silk suture (Henry Schein, Melville, NY) was passed through one end of the tissue section 3 mm below the cut edge, with the other attached to the test rig. Samples were preloaded with 0.05 N stress at 5 mm/min. Data were then recorded at a continuous extension rate of 5 mm/min until tissue failure.

Glucose mass transfer

Mass transfer of glucose across the 0.75 mm dissected iHUA was assessed to determine if glucose transport was rate limiting for cell growth and proliferation. Using the same experimental design as the cell seeded constructs, nonseeded HUA ($n = 3$) were assembled into the bioreactors. The tube-side flow circuit was continuously perfused with deionized water (total volume of 4.4 mL), at a flow rate of 0.3 mL min^{-1}. The shell-side was perfused with a 5.5*M* glucose solution (total volume 4.4 mL) at the same flow rate. Glucose quantification was assessed by sampling 50 μL aliquots at 30 min and 1 h intervals over a 5 h period. Glucose concentration was assessed using hexokinase-glucose 6-phosphate dehydrogenase based assay.

To calculate glucose permeability through the 0.75 mm iHUA, the flowing equation was used assuming quasi steady state[21,22]:

$$\ln\left(\frac{C_0 - 2C_t}{C_0}\right) = -\left(\frac{A}{V}P\right)t$$

where C_t is the concentration in the lumenal flow measured at any time t, C_0 is the initial concentration of glucose in the ablumenal side, A (cm^2) is the materials surface area, V (in mL) is the volume flowed in the lumenal void and P (cm s^{-1}) is the permeability of the material. The logarithmic expression given above was calculated for each time point by measuring C_t and plotted as a function of time. The slope, from which the permeability was deduced, was obtained by a linear fit.

The flux J (g cm^{-2} s^{-1}) was deduced from the permeability assuming an initial exterior glucose concentration of 4.5 mg/mL, a membrane width of 0.75 mm, and using the following formula:

$$J = P\,\frac{dC}{dx}$$

Using an average surface area of the material of 3.15 cm^2 (3.5 $\times$ 0.9 cm^2), the total flux of glucose was calculated.

Histology

All tissue samples were fixed a 3% buffered formal saline for 12 h prior to dehydration and imbedding. Histology samples were sectioned (7 μm) and stained with hematoxylin 7211 (Richard-Allan Scientific, Kalamazoo, MI), then counter stained with Eosin-Y (Richard-Allan Scientific) using standard protocols. Tissue structure and cellu-

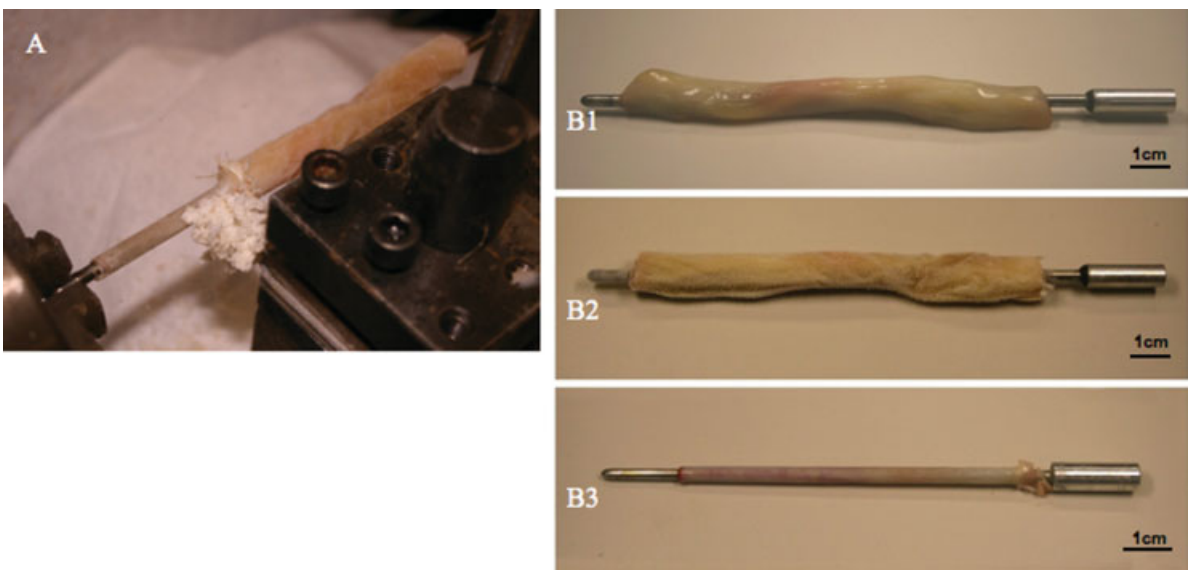

Figure 2. Automated dissection of the human umbilical artery: (A) shows the machining process midway through dissection, with (B1) showing the umbilical cord mounted on a stainless steal mandrel, frozen to −80°C (B2) then machined at a longitudinal speed of 5 mm/s, resulting in a smooth homogenous tubular material, (B3). [Color figure can be viewed in the online issue, which is available at www.interscience.wiley.com.]

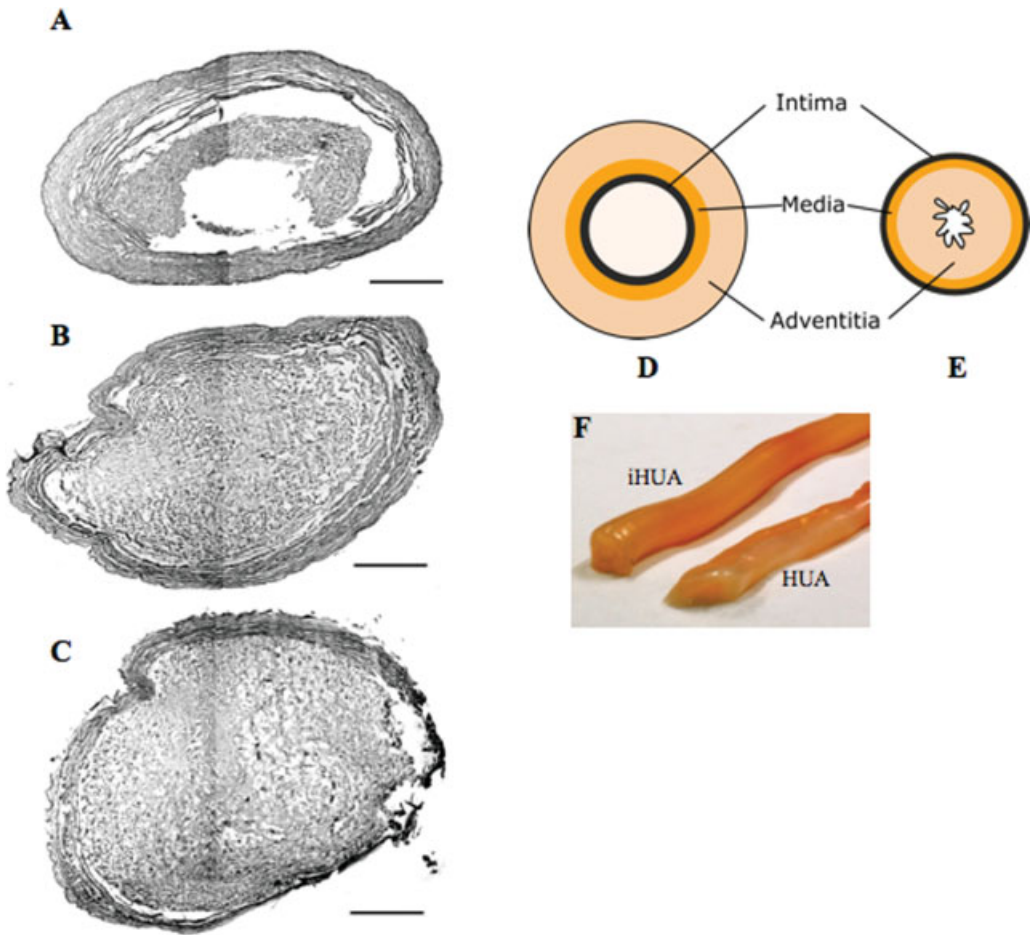

Figure 3. Orientation of the HUA and iHUA: The normal orientation of the HUA (D) is reversed using arthroscopy forceps, inverting the natural layered organization of the material (E). Histological section of arteries after lathing and inversion for three cutting thickness are shown in (A) 0.25 mm, (B) 0.5 mm, (C) 0.75 mm, scale bar is 500 μm. Photographs of lathed and inverted (iHUA) or native (HUA) arteries are shown in (D). [Color figure can be viewed in the online issue, which is available at www.interscience.wiley.com.]

lar composition were assessed using an E800 Nikon light microscope.

SEM

Decellularized HUA was cut open longitudinally and fixed overnight in 1% (v/v) glutaraldehyde in PBS (Sigma). Samples were washed in PBS and fixed in 1% osmium for 2 h. After a final wash, the samples were dehydrated in graded ethanol (30, 50, 70, 90, 95, and 100% (v/v) for 10 min each) before being critical point dried in CO_2 (Autosamdri-814, Tousimis, Rockville, MD). Samples were then mounted, carbon spotted to enhance the conductivity; gold sputtered and analyzed using the JEOL JSM-880 SEM.

RESULTS

HUA dissection and decellularization

The automated dissection procedure is a rapid process, requiring less than 2 min to dissect a section of the artery from the bulk cord.[23] This method allows precise control over the wall thickness of the tubular material by adjusting the lathe's cutting depth, resulting in a tubular structure with a smooth uniform surface, see Figure 2(A,B). Figure 3(D) displays the normal, and inside–out orientations Figure 3(E) of the HUA scaffold, with Figure 3(F) showing the more rigid shape of the iHUA compared to the normally orientated vessel that collapses. The process of turning the HUA inside out varies in difficulty as a function of the wall thickness, where increased wall thicknesses compress more tissue within the lumen. Initial testing with samples machined with wall thickness $>$0.75 mm resulted in a majority of vessels splitting. For this reason, wall thicknesses of 0.25, 0.50, and 0.75 mm were assessed, see Figure 2(A,B,C). Figure 4(A) shows the increased compression effect within the iHUA as the wall thickness increases, with a pictorial representation shown in Figure 3(B).

The decellularization process removed residual blood, cells, and other soluble components of the scaf-

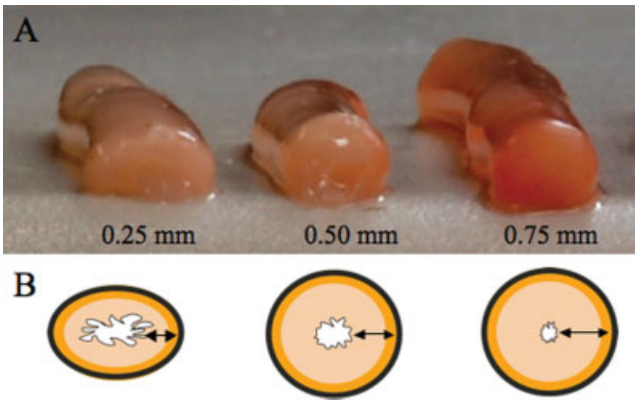

Figure 4. iHUA structure after lathing and thawing: Machining differences wall thicknesses of the HUA results in increased, or decreased compression of the Wharton's jelly within the *neo*-lumen. The iHUA with walls machined to 0.25 mm, behaved similar to the HUA in its natural orientation, and were found to collapse after lathing. Whereas vessels machined to 0.5 and 0.75 mm were more rigid, maintaining tubular form. (A) shows the inverted vessels (iHUA), with (B) illustrating the effect of increased wall thickness on the lumenal void. [Color figure can be viewed in the online issue, which is available at www.interscience.wiley.com.]

fold, changing the color from a light red/brown to white. Typical of SDS based decellularization methods a degree of disruption in the ECM was noted, particularly in the vessels medial layer. Structural deformation in ECM fiber alignment was confirmed by SEM analysis with the native ECM showing aligned fibers compared to the relative disorganized structure of the decellularized HUA, see Figure 5(A cellular, B decellularized). Histology shows a basement membrane void of endothelial cells with no obvious cellular structures (nuclei) present within the vessels medial layer. Similarly, the dispersed fibroblast-like cells that populate the Wharton's jelly are no longer evident, see Figure 5(C cellular, D acellular) HUA.

SEM analysis of the decellularized vessels with each of the three wall thicknesses (0.25, 0.50, and 0.75 mm), show the typical surface topography of the lumenal basement membrane, with the ablumenal surface displaying a more fibrous morphology. Occasionally, a slight tearing of the basement membrane (BM) on the lumenal surface was noted, where the membrane appears to have lifted off the underlying lamina, these morphologies were noted on all

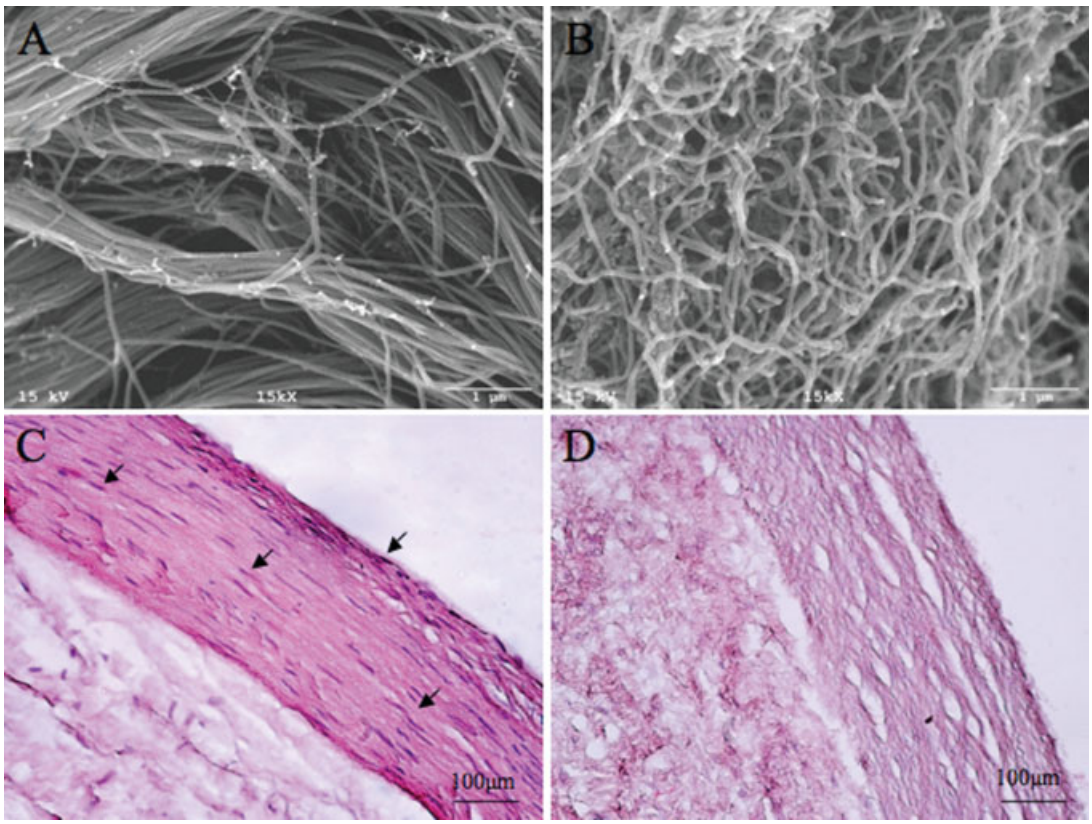

Figure 5. Effect of the decellularization process on the HUA. SEM analysis shows the adventitial surface morphology before decellularization (A), with (B) showing some disruption of the adventitial fiber organization by the decellularization process. Similarly, histology shows structural denaturation before (C) and after (D) decellularization. Arrows indicate cells removed by the decellularization step. [Color figure can be viewed in the online issue, which is available at www.interscience.wiley.com.]

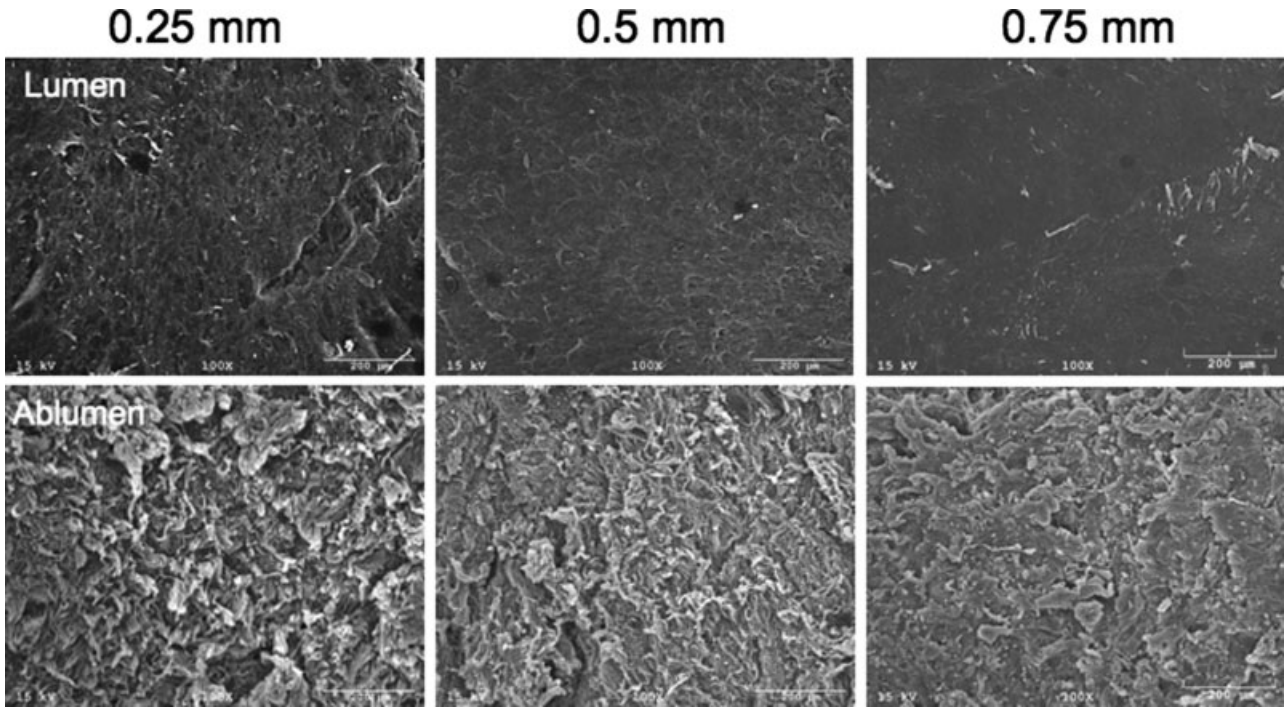

Figure 6. SEM analysis of the lumenal and ablumenal surfaces: Lumenal (top) and ablumenal (bottom) surfaces were analyzed for the three wall thicknesses assessed here (0.25, 0.5, and 0.75 mm). No significant variation was noted in the decellularized lumenal surface between each of the different wall thicknesses. Observations of the ablumenal surface, composed predominantly of type I collagen ECM (lathed surface), was found to have a less uniform, rougher structure, relative to the lumenal side.

samples (0.25, 0.50, and 0.75 mm), although a qualitative assessment indicated the 0.25 mm samples to have marginally more BM disruption. No observable variation was noted of the ablumenal surface between the three different thicknesses, see Figure 6.

Mechanical properties

Stress–strain analysis (in the longitudinal orientation) on the three different HUA wall thicknesses (0.25, 0.5, and 0.75 mm) after decellularization, resulted in a typical biphasic curve for soft tissues. Showing an elastic toe region leading to the inflexion point before a liner region of increased stiffness prior to tissue failure, see Figure 7. The force at ultimate failure increased with increasing wall thickness, however the stress at failure (force divided by the initial cross sectional area), was statistically independent of wall thickness; however, the 0.25 mm scaffold had, on average, higher mean values indicating the anisotropic nature of the scaffold wall as the ratio of Wharton's jelly increases. Similarly the mean strain at failure (33% ± 5%) also independent of the vessels thickness. The toe region was significantly more elastic than at higher strain values (10–30%) where stiffness was 10–25 times higher than the toe region, see Table I.

Suture retention in the longitudinal orientation, indicated a peak force required to tear the suture from the tissue. Results show the suture retention values at 74.67 ± 4.93 N for the 0.25 mm HUA, 116.33 ± 11.59 N for the 0.5 mm HUA and 168 ± 11.53 N for the 0.75 mm HUA. A statistically signifi-

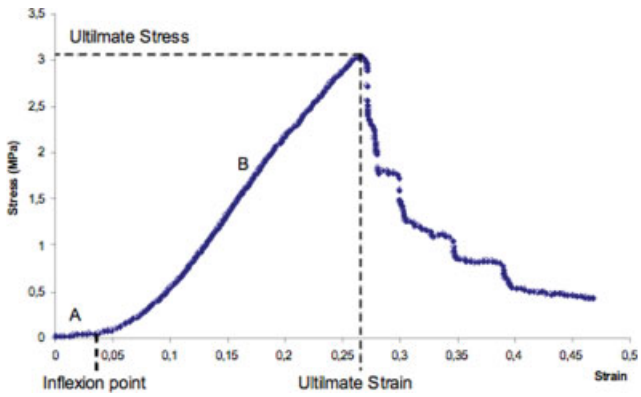

Figure 7. Representative longitudinal stress–strain curve for the human umbilical artery. The ultimate stress (stress at failure), ultimate strain (strain at failure) along with two stiffness measurements: before the point of inflexion in the "toe region" (A) and in the more traditional linear region (B) are calculated to characterize the material. [Color figure can be viewed in the online issue, which is available at www.interscience.wiley.com.]

TABLE I
Tensile Analysis

Mechanical Properties						
Wall Thickness (mm)	Force at Failure (N)	Stress at Failure (MPa)	Strain at Failure (% strain)	Point of Inflexion (%)	Stiffness (MPa)	
					A	B
0.25	8.87 ± 1.85	3.47 ± 0.72	33 ± 4	2.67 ± 0.17	0.83 ± 0.13	16.04 ± 1.94
0.50	13.82 ± 2.47	2.71 ± 0.48	34 ± 5	1.01 ± 0.65	0.55 ± 0.1	13.31 ± 2.59
0.75	22.01 ± 3.65	2.87 ± 0.47	34 ± 7	2.04 ± 0.83	1.53 ± 1.07	14.25 ± 3.51

NOTE: The force at ultimate failure increases with increasing adventitia thickness, showing its role in the HUA's longitudinal strength. Stress at failure was obtained by dividing the force by the cross-sectional area of the material; no variation with wall thickness was noticed ($p < 0.05$). Strain at failure was measured at around 30% of initial length, and this value fits in the low range of the ultimate strain fresh peripheral nerves can undergo. The point of inflexion was used to calculate the stiffness in the "toe region" (A), the stiffness in the linear region was also calculated (B). Stiffness in the linear region is more than 10 times greater than in the toe region. Both yielded some variation between thicknesses.

cant increase in the ultimate failure was noted as the wall thickness increased, indicating the amorphous Wharton's Jelly provides a degree of mechanical support. ($p < 0.05$), see Figure 8.

Glucose permeability

The perfusion circuit was initiated with a concentration profile of glucose diffusing from the shell-side flow circuit into the tube-side was found to be linear when plotted as a function of time, with all correlation coefficients above 0.96 (data not shown). The average permeability for glucose obtained was $1.34 \times 10^{-4} \pm 0.18 \times 10^{-4}$ cm s^{-1} at 37°C. Glucose flux in an average size artery was found to be ~1.89 μg s^{-1}. As a comparison, PC12 cells in culture plate have a consumption rate of in the range of 5.2×10^{-3} pg s^{-1} $cell^{-1}$ (data not shown).

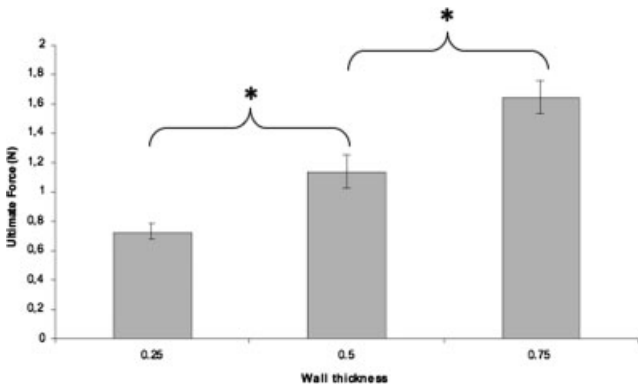

Figure 8. Suture retention: As the wall thickness increased suture retention also increased (*$p < 0.05$). Performed on a flat sheet of the HUA with a suture 3 mm from the tissue edge, sutures failure occurred from 0.73 ± 0.05 N for the 0.25 mm HUA to 1.65 ± 0.11 N for the 0.75 mm HUA. Increasing force with wall thickness suggests that the adventitia plays a critical role for suture retention strength.

Cellular interactions

Histology of the 0.75 mm iHUA after 2 weeks culture with PC12 cells seeded within the *neo*-lumen showed cellular adhesion on the material with cells surrounding the edge of the adventitia, see Figure 10. Cellular invasion into the iHUA wall was also noted, with aggregates of cells observed within the scaffold. This cellular invasion was accompanied with an increase in glucose consumption after a 7–8 days lag period, see Figure 9. After 2 weeks, some of the matrix present in the lumen was degraded and voids between cells aggregates were observed. Controls with no cells showed no degradation of the matrix suggesting the role of the PC12 in this degradation process.

DISCUSSION

The human umbilical cord contains two arteries and a vein, surrounded by connective tissue called

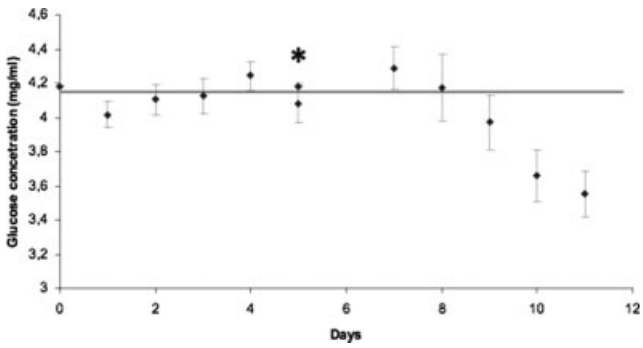

Figure 9. Glucose consumption during perfusion culture: PC12 neuronal-like cells cultured within the iHUA mounted in the bioreactors displayed little detectable consumption during an initial lag period up to day 7–8 form controls (no cells) at 4.18 mg/mL. After this lag period a significant increase in glucose consumption is note, indicating increased cell function/proliferation within the scaffold.

Wharton's jelly. To produce a mechanically uniform material with a defined wall thickness, in a suitable time frame, a modified lathing technique was used to isolate the artery from the umbilical cord. The automated dissection technique developed here, is a rapid process (2–3 min), which allows for a precisely dialed-in scaffold wall thickness.

Because of its future *in vivo* applications, dissected scaffolds were decellularized to minimize immunoreactivity. SDS was used as the primary decellularizing agent as it has been shown to effectively remove cellular components of *ex vivo* materials.[24–26] However, SDS can be problematic to remove from the tissue, and as such EtOH rinses were used to enhance the extraction of organic compounds and facilitate SDS extraction.[16] Because most of the cellular content of the HUA lies within the intimal and medial layers, turning the artery inside out (iHUA) before decellularization may also enhance this extraction process by exposing these regions more effectively to decellularizing solutions. The decellularization process was shown to effectively reduce cellular content as observed by histology, however immunological acceptance is yet to be proven.

With the artery inside out, the Wharton's jelly is directly exposed to the seeded cells within the scaffold. The composition of Wharton's jelly is complex, and has been the subject of many histological studies. Jaworski et al. in 1996 studied the histology of the extracellular components of the human umbilical cord, finding it very rich in collagen (mostly type VI but also types I, III, IV, and V) and glycosaminoglycans (predominantly hyaluronic acid and sulphated GAGs).[27] The ultrastructure of the human umbilical showed to be organized in a network of microfibrils and surrounded by a mixture of basement membrane molecules such as laminin, heparan sulphate, and proteoglycans, and solubilized components such as salts and plasma proteins such as growth factors.[28–32] From a composition perspective, many of these molecules may have beneficial effect on neuronal growth. Laminin and type IV collagen are components of the Schwann cell basal membrane, and have been shown to play an important role in neurite outgrowth in peripheral nerve injuries.[33–35] Heparan sulphate proteoglycans have also shown to have and important role in axonal development,[36,37] thought to be a messenger for axonal growth triggering[38] and may also have the role of nerve growth factor storage.[39] Finally, hyaluronic acid might also influence nerve repair because of its interactions with unmyelinated nerve fibers.[34]

Three different scaffold wall thicknesses have been assessed here, each showing potential as a grafting material. Evidence suggests the size of the lumen to be a critical parameter for *in vivo* nerve regeneration,[40] and as such it will be necessary to further optimize the lumenal size by altering the Wharton's jelly content to identify the ideal conditions that promote regeneration. An excessively small lumen may inhibit cell migration and neurite elongation as the ECM would form a barrier that would need to be degraded, and remodeled in order for neurons to bridge the defect. An excess of the Wharton's jelly may also inhibit diffusion of larger molecules, including neurotrophic factors, thus limiting the regeneration potential. Conversely, if the Wharton's jelly is not compressed sufficiently within the core of the scaffold structural collapse may occur. In addition, if the total wall thickness is too thin fibroblasts can infiltrate causing scar tissue formation, and growth factors may diffuse out of the regenerative environment.[3] Controlling the cutting thickness during the lathing process allows a degree of tuning that alters the amount of Wharton's jelly left on the artery.

Under physiological conditions, joint movement places peripheral nerves under tensile stress. *In vivo* studies have shown that most peripheral nerves elongate 3–10%,[41] with some nerves such as the ulnar nerve extend up to 30% of their initial length with a 90° elbow abduction.[42] Above physiological strain values, nerves cease to function properly, primarily due to a reduced blood supply.[43,44] Longitudinal stress strain analysis has shown a biphasic curve, with a more elastic toe region between 8 and 10% strain, from which stiffness increases rapidly until tissue failure. These mechanical properties are well adapted to the physiological conditions, where normal physiological strains remains in the more elastic toe region, only elongating into the stiffer region under extreme conditions.[41]

Ideally, a defect bridging material would have mechanical properties that resemble those of the original fresh nerve tissue it's replacing. These investigations have shown the iHUV to have broadly similar mechanical properties, with a biphasic stress–strain analysis. Depending on the wall thickness, the HUA scaffold has a more elastic toe region between 1 and 2.5% strain, with strain values up to 33.03% ± 0.53%, independent of wall thickness for the decellularized iHUA. As a comparison, the rabbit tibia1 nerve has an ultimate strain of 38.5% ± 0.02%.[45] The maximal tensile stress for nerves can range from 2.7 to more than 10 MPa,[46,47] depending on the specific nerve and it's origin. The iHUA was found to have a ultimate tensile stress of 3.02 ± 0.4 MPa, independent of the wall thickness. Although stress values are at the lower end of the physiological stress range it is likely to be satisfactory considering the extreme physiological strain needed to reach such stress. The relationship between wall thickness and ultimate force indicates that the connective tissues within the Wharton's jelly layer contributes significantly to the

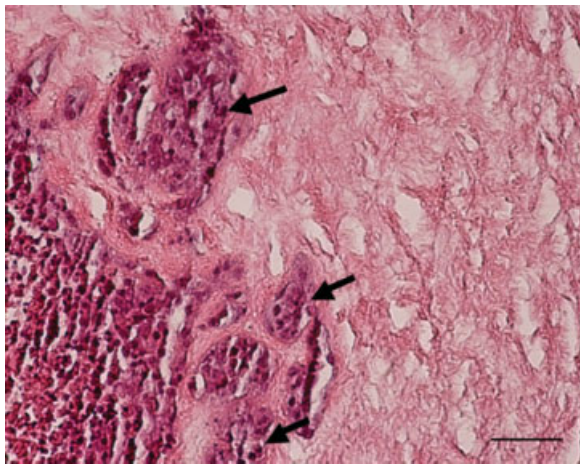

Figure 10. PC12 cell culture within the 0.75 mm iHUA: Histological results show after 11 days culture seeded PC12 cells appear to have adhered around the lumenal void, with cells integrating with the preexisting iHUA scaffold (black arrows). Some void areas are noted between cell aggregates, with possible cell–scaffold remodeling occurring. [Color figure can be viewed in the online issue, which is available at www.interscience.wiley.com.]

axial mechanical strength, with SEM images showing a majority ECM fibers to be radially oriented. This orientation is well adapted for physiological conditions in a blood vessel, and is thought to be responsible for the lower axial strain values at failure. The ability of the processed iHUA scaffold to retain sutures under applied force is an important parameter for surgical handling of the material. Suture retention was expressed in force with results showing the more adventitia/Wharton's jelly present (thinker materials), the higher the force values at the point of failure.

Glucose diffusion through the iHUA is an essential requisite if this material is support cells within the lumen. Within the bioreactors, media was perfused through the shell-side circuit, in contact with the outer artery wall, with passive diffusion of the mechanism of nutrients transport. The material is decellularized to remove immunogenic cells and other soluble components of the matrix, enhancing permeability. Glucose transport was assessed in order to determine if sufficient glucose could penetrate the scaffold wall to maintain a cell population within the artery. Results show that the flow of glucose through the material is sufficient to support the growth. However, with the intima and medial layers having a more dense ECM structure, relative to the adventitial layer, these layers may inhibit transport of larger molecules not assayed. However cells were shown to remain viable within the scaffold up to 2 weeks as shown by progressive glucose consumption. Only the 0.75 mm scaffold was assessed as the permeability of 0.5 and 0.25 mm iHUA will be greater than, or equal to the 0.75 mm scaffold.

CONCLUSION

We present herein, a novel material, to our knowledge undescribed in the literature, and demonstrate its suitability as a scaffold and ECM for cell growth and function support. After 2 weeks culture of the seeded construct, the iHUA showed the ability of this material to support PC12 cells. Cells were seen to migrate into the scaffold, as seen in Figure 10. Biocompatibility and cell adhesion has been established here, although further optimization is required to obtain a more uniform cellular distribution within the scaffold if it is to be used in an *in vitro* system. The iHUA has shown to be a promising candidate for nerve tissue engineering. By inverting the original orientation of this multi layered material, a favorable matrix for cell adhesion and potentially for neuronal proliferation and elongation is exposed to the invading cells and prevents the structures from collapsing. The automated dissection technique shows promise for scale-up with a rapid process time compared to manual dissection, and minimizes natural variability. The HUA's material and structural properties show potential for an usage as a guidance channel as well as for *in vitro* culture in a bioreactor, however determining the ideal wall thickness that prevents collapse and allows complete cellular development requires further investigation. By using this tubular scaffold and bioreactor system, investigations assessing neuronal growth factors, electrical stimulation and other environmental factors become possible. A step closer to functional engineered nerves.

References

1. Ciardelli G, Chiono V. Materials for peripheral nerve regeneration. Macromol Biosci 2006;6:13–26.
2. Lee AC, Yu VM, Lowe JB III, Brenner MJ, Hunter DA, Mackinnon SE, Sakiyama-Elbert SE. Controlled release of nerve growth factor enhances sciatic nerve regeneration. Exp Neurol 2003;184:295–303.
3. Hudson TW, Evans GR, Schmidt CE. Engineering strategies for peripheral nerve repair. Orthop Clin North Am 2000;31:485–498.
4. Chiu DT, Janecka I, Krizek TJ, Wolff M, Lovelace RE. Autogenous vein graft as a conduit for nerve regeneration. Surgery 1982;91:226–233.
5. Suematsu N, Atsuta Y, Hirayama T. Vein graft for repair of peripheral nerve gap. J Reconstr Microsurg 1988;4:313–318.
6. Chiu DT, Strauch B. A prospective clinical evaluation of autogenous vein grafts used as a nerve conduit for distal sensory nerve defects of 3 cm or less. Plast Reconstr Surg 1990;86:928–934.
7. Dellon AL. Wound healing in nerve. Clin Plast Surg 1990;17:545–570.
8. Fields RD, Le Beau JM, Longo FM, Ellisman MH. Nerve regeneration through artificial tubular implants. Prog Neurobiol 1989;33:87–134.
9. Wang KK, Costas PD, Bryan DJ, Jones DS, Seckel BR. Inside-out vein graft promotes improved nerve regeneration in rats. Microsurgery 1993;14:608–618.

10. Ferrari F, De Castro Rodrigues A, Malvezzi CK, Dal Pai Silva M, Padovani CR. Inside-out vs. standard vein graft to repair a sensory nerve in rats. Anat Rec 1999;256:227–232.
11. Wang KK, Costas PD, Bryan DJ, Eby PL, Seckel BR. Inside-out vein graft repair compared with nerve grafting for nerve regeneration in rats. Microsurgery 1995;16:65–70.
12. Kelleher MO, Al-Abri RK, Eleuterio ML, Myles LM, Lenihan DV, Glasby MA. The use of conventional and invaginated autologous vein grafts for nerve repair by means of entubulation. Br J Plast Surg 2001;54:53–57.
13. Benito-Ruiz J, Navarro-Monzonis A, Piqueras A, Baena-Montilla P. Invaginated vein graft as nerve conduit: An experimental study. Microsurgery 1994;15:105–115.
14. Bungner OV. Ueber die degenerations und regenerations-Vorgange am nerven nach verletzungen. Beirtr Pathal Anal 1891;10:321.
15. Barcelos AS, Rodrigues AC, Silva MD, Padovani CR. Inside-out vein graft and inside-out artery graft in rat sciatic nerve repair. Microsurgery 2003;23:66–71.
16. Gratzer PF, Harrison RD, Woods T. Matrix alteration and not residual sodium dodecyl sulfate cytotoxicity affects the cellular repopulation of a decellularized matrix. Tissue Eng 2006; 10:2975–2983.
17. Brown B, Lindberg K, Reing J, Stolz DB, Badylak SF. The basement membrane component of biologic scaffolds derived from extracellular matrix. Tissue Eng 2006;12:519–526.
18. McFetridge PS, Bodamyali T, Chaudhuri JB, Horrocks M. Endothelial and smooth muscle cell seeding onto processed ex vivo arterial scaffolds using 3D vascular bioreactors. ASAIO J 2004;50:591–600.
19. McFetridge PS, Daniel JW, Bodamyali T, Horrocks M, Chaudhuri JB. Preparation of porcine carotid arteries for vascular tissue engineering applications. J Biomed Mater Res 2004; 70A:224–234.
20. Courtman DW, Pereira CA, Omar S, Langdon SE, Lee JM, Wilson GJ. Biomechanical and ultrastructural comparison of cryopreservation and a novel cellular extraction of porcine aortic valve leaflets. J Biomed Mater Res 1995;29:1507–1516.
21. Truskey G, Yuan F, Katz D. Transport Phenomena in Biological Systems. Upper Saddle River, NJ: Pearson Prentice Hall; 2004. p 317–321.
22. Raghavan D, Kropp BP, Lin HK, Zhang Y, Cowan R, Madihally SV. Physical characteristics of small intestinal submucosa scaffolds are location-dependent. J Biomed Mater Res A 2005;73:90–96.
23. Daniel J, Abe K, McFetridge PS. Development of the human umbilical vein scaffold for cardiovascular tissue engineering applications. Asaio J 2005;51:252–261.
24. Martin ND, Schaner PJ, Tulenko TN, Shapiro IM, Dimatteo CA, Williams TK, Hager ES, DiMuzio PJ. In vivo behavior of decellularized vein allograft. J Surg Res 2005;129:17–23.
25. Rieder E, Kasimir MT, Silberhumer G, Seebacher G, Wolner E, Simon P, Weigel G. Decellularization protocols of porcine heart valves differ importantly in efficiency of cell removal and susceptibility of the matrix to recellularization with human vascular cells. J Thorac Cardiovasc Surg 2004;127:399–405.
26. Gilbert TW, Sellaro TL, Badylak SF. Decellularization of tissues and organs. Biomaterials 2006;27:3675–3683.
27. Bankowski E, Sobolewski K, Romanowicz L, Chyczewski L, Jaworski S. Collagen and glycosaminoglycans of Wharton's jelly and their alterations in EPH-gestosis. Eur J Obstet Gynecol Reprod Biol 1996;66:109–117.
28. Takechi K, Kuwabara Y, Mizuno M. Ultrastructural and immunohistochemical studies of Wharton's jelly umbilical cord cells. Placenta 1993;14:235–245.
29. Vizza E, Correr S, Goranova V, Heyn R, Angelucci PA, Forleo R, Motta PM. The collagen skeleton of the human umbilical cord at term. A scanning electron microscopy study after 2N-NaOH maceration. Reprod Fertil Dev 1996;8:885–894.
30. Nanaev AK, Kohnen G, Milovanov AP, Domogatsky SP, Kaufmann P. Stromal differentiation and architecture of the human umbilical cord. Placenta 1997;18:53–64.
31. von Kaisenberg CS, Krenn V, Ludwig M, Nicolaides KH, Brand-Saberi B. Morphological classification of nuchal skin in human fetuses with trisomy 21, 18, and 13 at 12-18 weeks and in a trisomy 16 mouse. Anat Embryol (Berl) 1998;197:105–124.
32. Sobolewski K, Malkowski A, Bankowski E, Jaworski S. Wharton's jelly as a reservoir of peptide growth factors. Placenta 2005;26:747–752.
33. Toyota B, Carbonetto S, David S. A dual laminin/collagen receptor acts in peripheral nerve regeneration. Proc Natl Acad Sci USA 1990;87:1319–1322.
34. Eggli PS, Graber W. Ultrastructural association of hyaluronan with rat unmyelinated nerve fibres. J Neurocytol 1996;25:79–87.
35. Siironen J, Sandberg M, Vuorinen V, Roytta M. Laminin B1 and collagen type IV gene expression in transected peripheral nerve: Reinnervation compared to denervation. J Neurochem 1992;59:2184–2192.
36. Eldridge CF, Sanes JR, Chiu AY, Bunge RP, Cornbrooks CJ. Basal lamina-associated heparan sulphate proteoglycan in the rat PNS: Characterization and localization using monoclonal antibodies. J Neurocytol 1986;15:37–51.
37. Mehta H, Orphe C, Todd MS, Cornbrooks CJ, Carey DJ. Synthesis by Schwann cells of basal lamina and membrane-associated heparan sulfate proteoglycans. J Cell Biol 1985;101:660–666.
38. Bulow HE, Berry KL, Topper LH, Peles E, Hobert O. Heparan sulfate proteoglycan-dependent induction of axon branching and axon misrouting by the Kallmann syndrome gene kal-1. Proc Natl Acad Sci USA 2002;99:6346–6351.
39. Halfter W. A heparan sulfate proteoglycan in developing avian axonal tracts. J Neurosci 1993;13:2863–2873.
40. Williams LR, Longo FM, Powell HC, Lundborg G, Varon S. Spatial-temporal progress of peripheral nerve regeneration within a silicone chamber: Parameters for a bioassay. J Comp Neurol 1983;218:460–470.
41. Topp KS, Boyd BS. Structure and biomechanics of peripheral nerves: Nerve responses to physical stresses and implications for physical therapist practice. Phys Ther 2006;86:92–109.
42. Wright TW, Glowczewskie F Jr, Cowin D, Wheeler DL. Ulnar nerve excursion and strain at the elbow and wrist associated with upper extremity motion. J Hand Surg [Am] 2001;26:655–662.
43. Clark WL, Trumble TE, Swiontkowski MF, Tencer AF. Nerve tension and blood flow in a rat model of immediate and delayed repairs. J Hand Surg [Am] 1992;17:677–687.
44. Tanoue M, Yamaga M, Ide J, Takagi K. Acute stretching of peripheral nerves inhibits retrograde axonal transport. J Hand Surg [Br] 1996;21:358–363.
45. Rydevik BL, Kwan MK, Myers RR, Brown RA, Triggs KJ, Woo SL, Garfin SR. An in vitro mechanical and histological study of acute stretching on rabbit tibial nerve. J Orthop Res 1990;8:694–701.
46. Borschel GH, Kia KF, Kuzon WM Jr, Dennis RG. Mechanical properties of acellular peripheral nerve. J Surg Res 2003;114: 133–139.
47. Millesi H, Zoch G, Reihsner R. Mechanical properties of peripheral nerves. Clin Orthop Relat Res 1995;(314):76–83.